Validation of GSMaP Data in Depicting Precipitation Climatology and Climate Variability in China

Zunya Wang * and Qingquan Li

Posted Date: 3 November 2023

doi: 10.20944/preprints202311.0169.v1

Keywords: GSMaP; station observations; validation; climatology; climate variability

Article

Validation of GSMaP Data in Depicting Precipitation Climatology and Climate Variability in China

Zunya Wang [1,*] and Qingquan Li [1,2]

[1] China Meteorological Administration Key Laboratory for Climate Prediction Studies, National Climate Center, Beijing China, 100081

[2] Collaborative Innovation Center on Forecast and Evaluation of Meteorological Disasters, Nanjing University of Information Science & Technology, Nanjing, China, 210044

* Corresponding author address: Zunya Wang, National Climate Center, China Meteorological Administration, Beijing, China E-mail: wangzy@cma.gov.cn.

Abstract: In this analysis, we assess the performance of GSMaP-GNRT6 data in capturing precipitation climatology and climate variability across China from 2001 to 2020. The evaluation involves comparing four precipitation indices of accumulated precipitation, the number of rainy days, rainstorm days and precipitation maximum with the daily precipitation data from 2419 stations of China. The findings reveal that the GSMaP data effectively captures the overall spatial distribution of annual, summer and monthly precipitation. However, its exhibits minor limitations in accurately depicting the spatial distribution of the number of rainy days from July to September and precipitation maximum during wintertime in eastern China. While the GSMaP data depicts a coherent annual cycle consistent with the station observations, a general underestimation is observed. Notably, the GSMaP data presents a much smoother annual cycle in precipitation maximum. Regarding accumulated precipitation, the number of rainstorm days, and precipitation maximum, the GSMaP data shows an almost consistent interannual variation and increasing trends, aligning with station observations. However, it is noteworthy that the magnitude of the increasing trend based on the GSMaP data is greater, especially entering the early 21st century. Conversely, a significant discrepancy in the annual variation and an almost opposite changing trend are noticed in the number of rainy days between the GSMaP data and station observations.

Keywords: GSMaP; station observations; validation; climatology; climate variability

1. Introduction

Precipitation stands as one of the most critical meteorological elements. As an integral component of global water and energy cycle, it not only signifies the prevailing local weather and climate conditions but also holds the potential to trigger meteorological disasters. Excessive precipitation tends to cause floods, mudslides, urban inundation and waterlogging [1–7], while unsufficient precipitation invariably results in drought [8–12]. Floods and droughts exert significant adverse impacts on agriculture, the economy and even human safety [13–18]. In particular, under the background of global warming, the intensity and frequency of precipitation extremes have increased greatly and caused severe damages to the society around the world [15,19–23]. Given that precipitation monitoring is vital for weather forecast and climate prediction, as well as further disaster prevention and mitigation, precipitation is of great challenging to estimate [24–32].

Station observations represent a primary method for conducting precipitation monitoring due to their high accuracy and real-time capabilities. However, the spatial resolution and homogeneity of meteorological monitoring are constrained by the scattered distribution of observations [31,33,34]. With the advancement of satellite remote sensing technology, related data are widely applied. On the one hand, satellite remote sensing data is utilized to generate reanalysis datasets [35,36]. Notably, two NCEP/NCAR reanalysis datasets (NCEP1 and NCEP2) [37,38], European Centre for Medium-Range Weather Forecasts (ECMWF) reanalysis data (ERA-40, ERA-Interim and ERA5) [39–42], the NCEP Climate Forest System Reanalysis system (CFSR) [43,44], and the Japanese 55-year Reanalysis

 doi:10.20944/preprints202311.0169.v1

(JRA-55) [45,46] are extensively utilized. On the other hand, satellite observations also can provide meteorological monitoring with high spatial resolution and extensive spatial coverage. Currently, various satellite precipitation datasets are available, such as CMORPH [47], the TRMM Multi-satellite Precipitation Analysis (TMPA) [48], PERSIANN [49–51], GSMaP [52,53], and others. To enhance the application of satellite precipitation, a series of validation and assessment studies have been conducted. Global and regional precipitation, particularly precipitation extremes, have been compared in numerous studies [32,33,46,54–56]. These studies report general spatial and temporal consistency and discuss the advantage and limitations of gauge-based precipitation, satellite estimation and reanalysis data.

The Global Satellite Mapping of Precipitation (GSMaP) is developed by the Japan Aerospace Exploration Agency (JAXA) [46,53], under the framework of the Global Precipitation Measurement (GPM), an international collaboration aimed at achieving highly accurate and frequent global precipitation observations [57,58]. GSMaP provides global precipitation estimates with a temporal resolution as high as 1 hour and a horizontal resolution of 0.1°. Its reliability has been extensively evaluated in various regions, such as Japan [53,59], the United States [53,60], mainland China [61–64], Australia [65] and Indonesia [66]. These studies demonstrate the primary accuracy of GSMaP and highlight biases in spatial distribution and magnitude in the climatology of daily or seasonal precipitation. To improve the monitoring of extreme precipitation, the World Meteorological Organization (WMO) initiated the Space-based Weather and Climate Extremes Monitoring (SWCEM) and a two-year (2018-2019) demonstration project, known as the WMO space-based weather and climate extremes monitoring demonstration project (SEMDP), conducted in the East Asia and Western Pacific region [67]. In this project, the generally good skill of GSMaP in monitoring extreme wet and dry events is validated through various case studies.

Despite of the relatively abundant researches on the validation of the GSMaP data, additional efforts are still required to address the shortcomings in current investigation. On one hand, existing outcomes are predominantly derived from case studies or short-term records, necessitating verification through more extended-term datasets. On the other hand, previous research has predominantly focused on climatology and daily or seasonal rainfall amounts, overlooking aspects such as climate variations and various precipitation indices. This analysis aims to fill these gaps by delving into a comprehensive evaluation of the GSMaP precipitation estimate over a 20-year period. Notably, China's complex terrain and diverse climate types, including the presence of the "third pole", the Tibetan Plateau, in western China, create challenges due to the combined impacts of the mid-latitude westerly wind and the East Asian monsoon [68–75]. Consequently, estimating precipitation based on satellite remains a significant challenge due to the intricate spatial distribution and temporal evolution of precipitation in the region. This study aims to provide valuable references for both the application and enhancement of GSMaP estimates.

The remainder of this analysis is structured as follows. Section 2 introduces the spatial coverage and research period of the GSMaP and the station observations in China, as well as the methods adopted. Section 3 illustrates the comparison of precipitation climatology between the two datasets. And the climate variation in precipitation by the two datasets is compared in Section 4. The main results are presented and discussed in Section 5.

2. Materials and Methods

In this analysis, the GSMaP Near-real-time Gauge-adjusted Rainfall Product version 6 (GSMaP_NRT_Gauge; GNRT6) is used [46]. It is the gauge-adjusted precipitation, provided within four hours after observation and updated at one-hour intervals. Hourly precipitation is available in this dataset, while we adopted the daily product from 1 Jan. 2001 to 31 Dec. 2020. This dataset covers a domain of 50.05°-239.95°E, 44.95°S-39.95°N, with a horizontal resolution of 0.1°×0.1°. Climatology is derived from 2001 to 2020 and annual and seasonal statistics are based on daily precipitation.

Using daily precipitation from 2419 national observation stations in China from 1 January 2001 to 31 December 2020, the GSMaP data were verified by comparing China's precipitation climatology and climate variability. This dataset is compiled by the National Meteorological Information Center

Preprints (www.preprints.org) | NOT PEER-REVIEWED | Posted: 3 November 2023 doi:10.20944/preprints202311.0169.v1

of the China Meteorological Administration, and primary quality control such as spatiotemporal consistency check and adjustment is carried out. To meet the requirements of climate analysis, two additional treatments are performed on the dataset. First, years in which the total number of missing records at a single station is greater than 20% are omitted. The second is to remove stations with continuous records of less than 15 years. Finally, 2378 stations are chosen for this analysis. For comparison with GSMap data, the station data is interpolated into a 0.1°×0.1° grid in the domain of 72.05°-123.95°E/18.05°-39.95°N.

In this analysis, a rainy day is defined as a day with daily precipitation equal to or greater than 0.1 mm, and a rainstorm day is defined as a day with daily precipitation equal to or greater than 50 mm. Climatology is an average from 2001 to 2020. Correlation analysis is adopted and statistical significance is tested using the student-t test. Also, the linear trend coefficient is calculated by the least squares method.

3. Results

3.1. Comparison of climatology

In this section, we compare the spatial distribution and annual cycle of mean precipitation, the number of rainy days, the number of rainstorm days, and precipitation maximum using GSMaP data and station observations. This validation aims to assess the capability of GSMaP in accurately representing the climatology of precipitation in China.

The annual precipitation pattern in China exhibits a decreasing from the southeast to the northwest, with a peak of up to 1800 mm in the southeast and no more than 200 mm in the northwest (Figure 1a). GSMaP data adeptly captures this spatial distribution, and the rainfall amount closely align with station observations (Figure 1b). However, some differences are noticeable (Figure 1c). GSMaP tends to underestimate precipitation to the south of the Yangtze River valley and in eastern Northwest China, while overestimating it in the middle and lower reaches of the Yellow River, western Northwest China and eastern Tibetan Plateau. Particularly noteworthy are the substantial biases around the Tibetan Plateau.

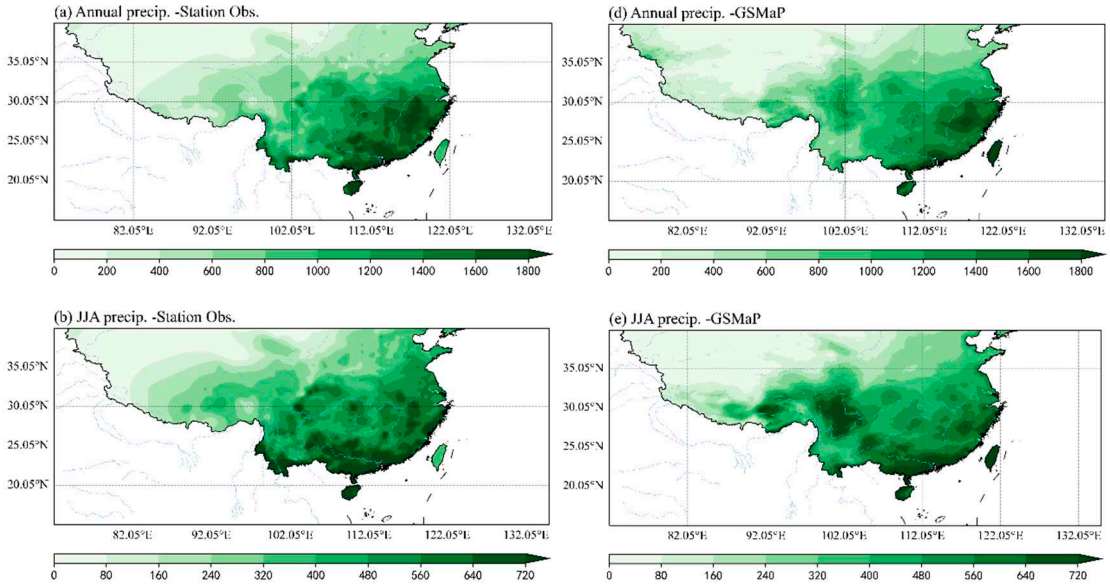

Preprints (www.preprints.org) | NOT PEER-REVIEWED | Posted: 3 November 2023 doi:10.20944/preprints202311.0169.v1

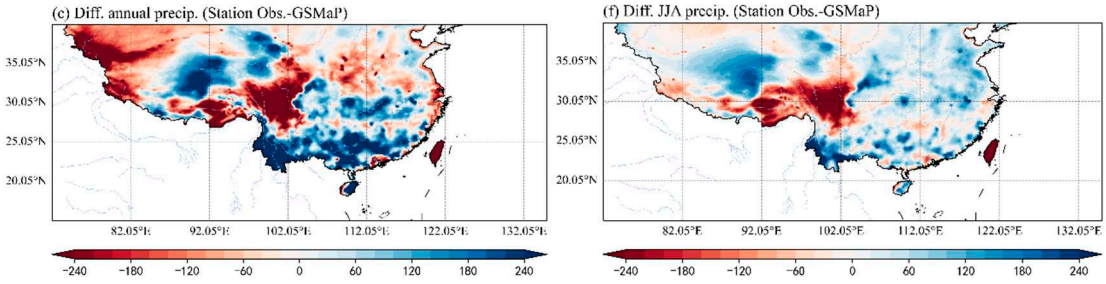

Figure 1. Distribution of annual (a and d, unit: mm) and summer (JJA, b and e) precipitation (b and e, unit: mm) across China based on station observations (a and b) and GSMaP data (d and e), and biases between station observations and GSMaP data (c and f, unit: mm; Station observations minus GSMaP data).

The precipitation in China predominantly occurs during the summer (JJA), showcasing a spatial distribution coherent with the annual precipitation pattern, and a peak exceeding 700 mm in the south coastal area (Figure 1d). GSMaP data accurately depicts this spatial distribution of summer precipitation (Figure 1e). Notably, positive biases in summer precipitation between GSMaP and station observations prevail over most of China, except for a pronounced negative bias centered in eastern and southern Tibetan Plateau (Figure 1f).

To quantitatively evaluate the ability of GSMaP to depict the spatial pattern of precipitation in China, monthly spatial correlations are calculated. As shown in Figure 2, the spatial correlation coefficients for each month consistently exceed 0.5, indicating that GSMaP data has a good ability to capture the spatial pattern of precipitation in China. And it can be noticed that correlations are relatively lower in January, February and November, hovering around or smaller below 0.6. In contrast, they are higher in the remaining months, peaking at 0.96 in May. Furthermore, GSMaP demonstrates a superior ability to represent the spatial distribution of precipitation in eastern China compared to the entire country, with all spatial correlations approximately or exceeding 0.8. Specifically, the similarity between GSMaP data and station observations is most pronounced from February to Jun, with spatial correlations surpassing 0.92 and reaching 0.96 in May and Jun. A comparison between China and eastern China suggests that GSMaP-based precipitation in western China is less consistent with station observations.

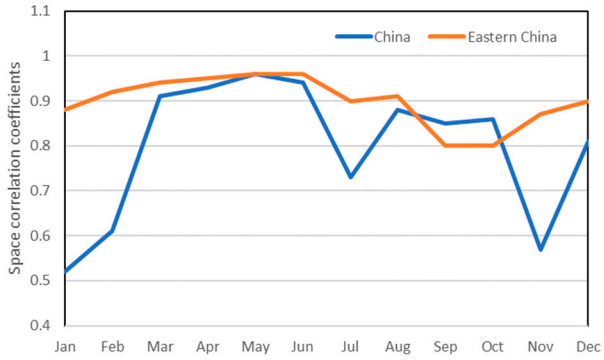

Figure 2. Spatial correlation coefficients of monthly climatic precipitation across China (blue line, 72.05°-122.55°E/17.55°-39.95°N) and eastern China (orange line, 105.05°-122.55°E/17.55°-39.95°N) between station observations and GSMaP data.

Precipitation in China is at its minimum during winter and peaks in summer, a seasonal cycle effectively depicted by GSMaP (Figure 3). Seen from Figure 3a, precipitation rises from January, attains its zenith in July and gradually diminishes until December, a trend consistent for both GSMaP and station observations. However, GSMaP data tends to be generally lower than station observations, with the largest disparity occurring in August, reaching an average difference of 32.5 mm across China. In eastern China, the annual cycle of precipitation exhibits significant alignment

Preprints (www.preprints.org) | NOT PEER-REVIEWED | Posted: 3 November 2023 doi:10.20944/preprints202311.0169.v1

between GSMaP and station observations. The primary distinction lies in GSMaP indicating higher precipitation in the first half of year compared to station observations. Furthermore, GSMaP places the precipitation peak occurs in Jun, contrasting with July in station observations. This further substrantiates that GSMaP more accurately captures the precipitation characteristics of in eastern China.

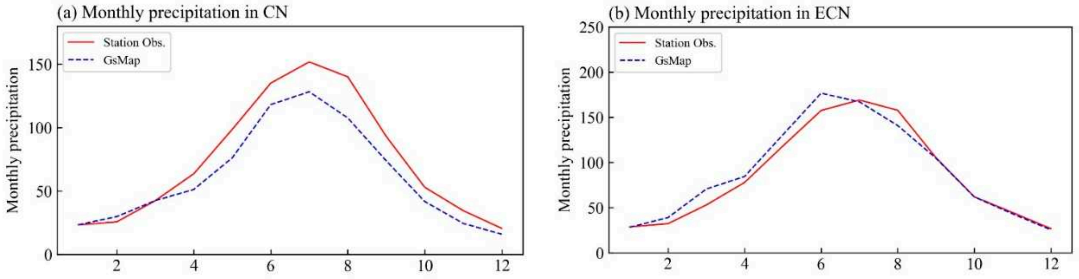

Figure 3. Climatological monthly precipitation averaged over China (a, unit: mm) and eastern China (b, unit: mm) based on station observations and GSMaP data.

Similar to the spatial distribution of precipitation, the number of rainy days in China exhibits a decreases from southeast to northwest, with high values extending from northeastern Tibetan Plateau to southern China (Figure 4a). GSMaP captures this trend, but the high-value belt is positioned father north, along the Yangtze River valley (Figure 4d). Due to this inconsistency in the high-value belt, the number of rainy days based on GSMaP is fewer than that based on station observation in southern China and most of the Tibetan Plateau, but greater in eastern Tibetan Plateau and north of the Yangtze River (Figure 4c). Additionally, the positive biases are generally larger than the negative deviations, suggesting an underestimation in the GSMaP data. In summer, the number of rainy days is concentrated in southwestern China, especially on the Tibetan Plateau, with some ares exceeding 70 days (Figure 4b). GSMaP data also exhibits a similar pattern, and its deviation pattern from station observations is coherent with that of the annual number of rainy days in China (Figure 4e and 4f).

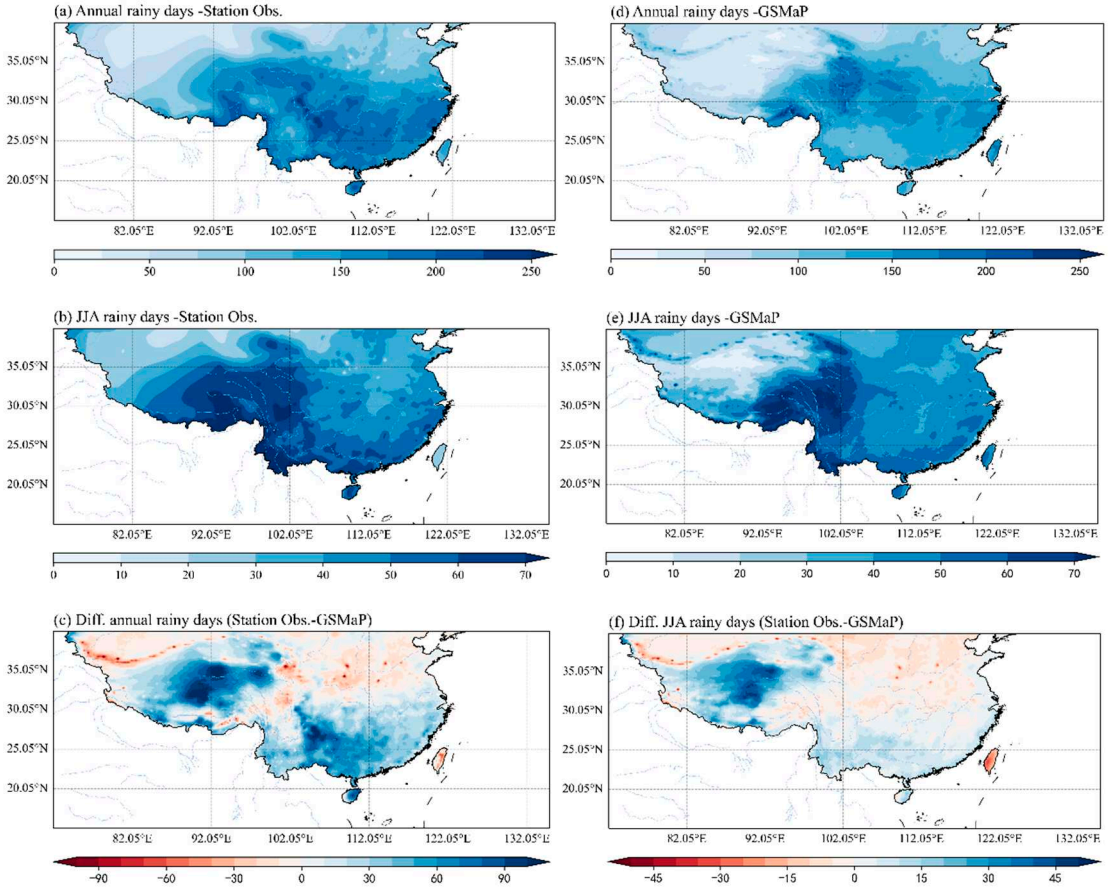

Preprints (www.preprints.org) | NOT PEER-REVIEWED | Posted: 3 November 2023 doi:10.20944/preprints202311.0169.v1

Figure 4. Distribution of annual (a and d, unit: days) and summer (JJA) number of rainy days (b and e, unit: days) across China based on station observations (a and b) and GSMaP data (d and e), and biases between station observations and GSMaP data (c and f, unit: days; Station observations minus GSMaP data).

The monthly spatial correlation of the number of rainy days in China between GSMaP and stations observations is stably around or greater than 0.7, with peaks in April and October reaching 0.84 (Figure 5). These high correlation coefficients affirm that GSMaP accurately represents the spatial distribution of the number of rainy days in China. Meanwhile, it can be noticed that the ability of GSMaP to depict the spatial pattern of the number of rainy days in eastern China varies by month. The correlation coefficients are generally higher in the first half of the year, exceeding 0.9 in May and Jun, but drop to smaller than 0.5 in September.

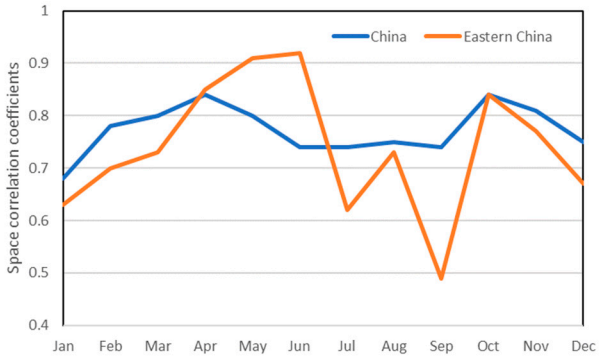

Figure 5. Spatial correlation coefficients of monthly climatic number of rainy days across China (blue line, 72.05°-122.55°E/17.55°-39.95°N) and eastern China (orange line, 105.05°-122.55°E/17.55°-39.95°N) between station observations and GSMaP data.

GSMaP effectively captures the annual cycle of an increase in the first half of the year and a decrease in the second half regarding the number of rainy days in China, with the peak occurring in July (Figure 6). Nevertheless, the number of rainy days derived from GSMaP data is consistently lower than that from station observations in each month, indicating a general underestimation in GSMaP, likely associated with the underestimation of precipitation. In eastern China, this underestimation by GSMaP is notably reduced and primarily occurs in winter months (Figure 6b).

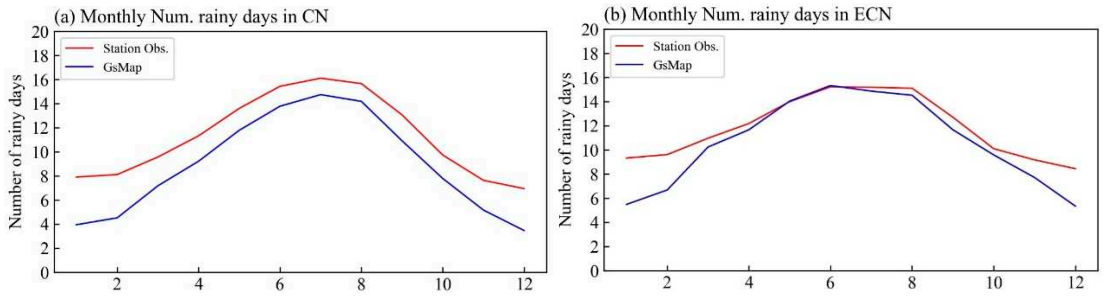

Figure 6. Climatological monthly number of rainy days averaged over China (a, unit: mm) and eastern China (b, unit: mm) based on station observations and GSMaP data.

As heavy rainfall predominantly occurs in the summertime, the focus is on the period from April to September in this analysis. Rainstorms are concentrated in southeastern China, particularly in south coastal areas, with the maximum annual number of rainstorm days reaching around 10 days (Figure 7a). However, rainstorm are infrequent in northern and western China. GSMaP data well captures both the spatial pattern and magnitude of this distribution (Figure 7d). In comparison, the number of rainstorm days is observed to be underestimated in most of eastern China but slightly overestimated in western China by GSMaP data (Figure 7c). The spatial distribution of the number of rainstorm days in summer mirrors that of the annual count, with high values situated in

Preprints (www.preprints.org) | NOT PEER-REVIEWED | Posted: 3 November 2023 doi:10.20944/preprints202311.0169.v1

southeastern China (Figure 7b). The number of rainstorm days derived from GSMaP appears to be less than station observations (Figure 7e), and further analysis supports this bias, revealing a pattern of "less in eastern China but more in western China" by GSMaP relative to station observations (Figure 7f). Monthly spatial correlations in the number of rainstorm days between GSMaP data and station observations are consistently higher than 0.8, reaching 0.9 in May for both the whole of China and eastern China (Figure 8). This high level of similarity indicates that GSMaP depicts the spatial patterns of severe precipitation well.

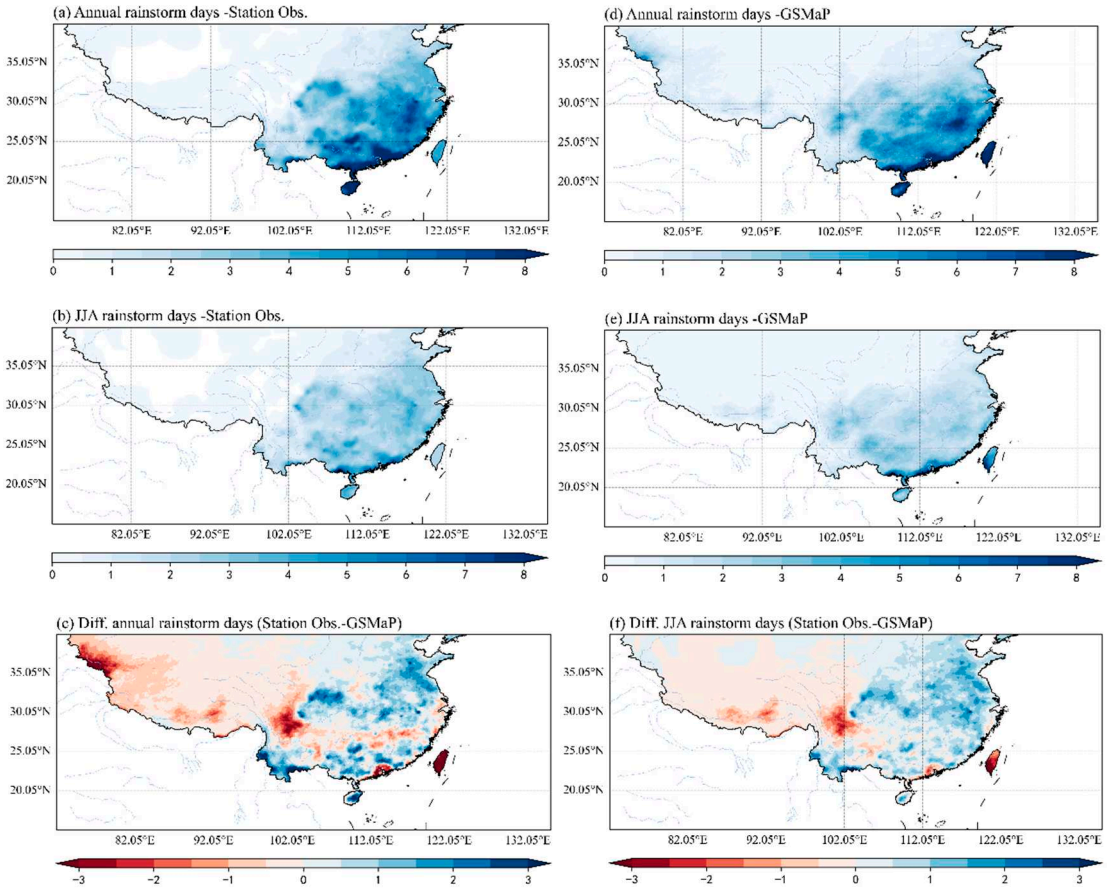

Figure 7. Distribution of annual (a and d, unit: days) and summer (JJA, b and e) number of rainstorm days (b and e, unit: days) across China based on station observations (a and b) and GSMaP data (d and e), and biases between station observations and GSMaP data (c and f, unit: days; Station observations minus GSMaP data).

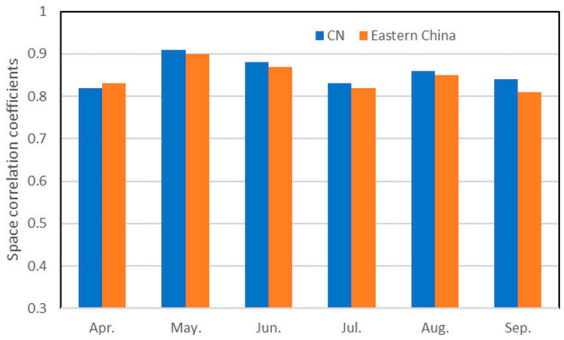

Figure 8. Spatial correlation coefficients of monthly climatic number of rainstorm days across China (blue bar, 72.05°-122.55°E/17.55°-39.95°N) and eastern China (orange bar, 105.05°-122.55°E/17.55°-39.95°N) between station observations and GSMaP data.

Preprints (www.preprints.org) | NOT PEER-REVIEWED | Posted: 3 November 2023 doi:10.20944/preprints202311.0169.v1

Rainstorms seldom occur during the winter months, gradually increasing from spring to summer and then decreasing thereafter (Figure 9). Both GSMaP data and station observations both capture this annual cycle. However, the temporal evolution of the number of rainstorm days also indicates an underestimation by GSMaP. In addition, the peak in the number of rainstorm days occurs earlier in GSMaP, specifically in May, compared to Jun in station observations.

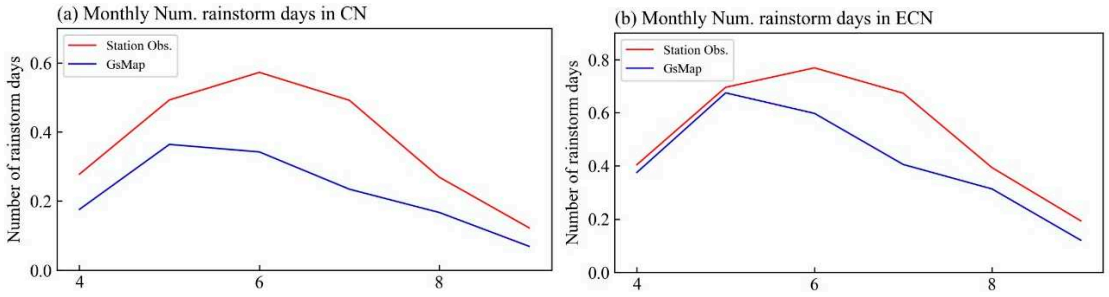

Figure 9. Climatological monthly number of rainstorm days averaged over China (a, unit: mm) and eastern China (b, unit: mm) based on station observations and GSMaP data.

The comparison of the maximum daily precipitation is undertaken to assess GSMaP's capability to depict extreme precipitation in this section. Climatologically, the daily precipitation maximum generally exceeds 80mm in eastern and southern China, as well as in a few locations in western China (Figure 10a). The scattered distribution of high values highlights the localized nature of precipitation, influenced by factors such as terrain height and small to medium-scale weather systems. GSMaP data demonstrates a similar spatial pattern of daily maximum precipitation in China (Figure 10b). The differences in precipitation maximum between station observations and GSMaP reveal a pattern of positive biases in most of eastern China and negative biases dominating western China. (Figure 10c). This pattern indicates underestimation in the east but overestimation in the west by GSMaP, similar to the situations observed for the number of rainy days and rainstorm days. Regarding monthly precipitation maximum in China, the spatial distribution discrepancy is substantial in January, with the spatial correlation being lower than 0.2 (Figure 11). However, in other months, the precipitation maximum from GSMaP shows a highly similar spatial pattern to that from station observations, with spatial correlations consistently around or above 0.7, reaching a peak exceeding 0.9 in May. The situation in eastern China comparable. And it can be noticed that the spatial correlation coefficients between GSMaP and station observations are generally lower than those observed for the entirety of China.

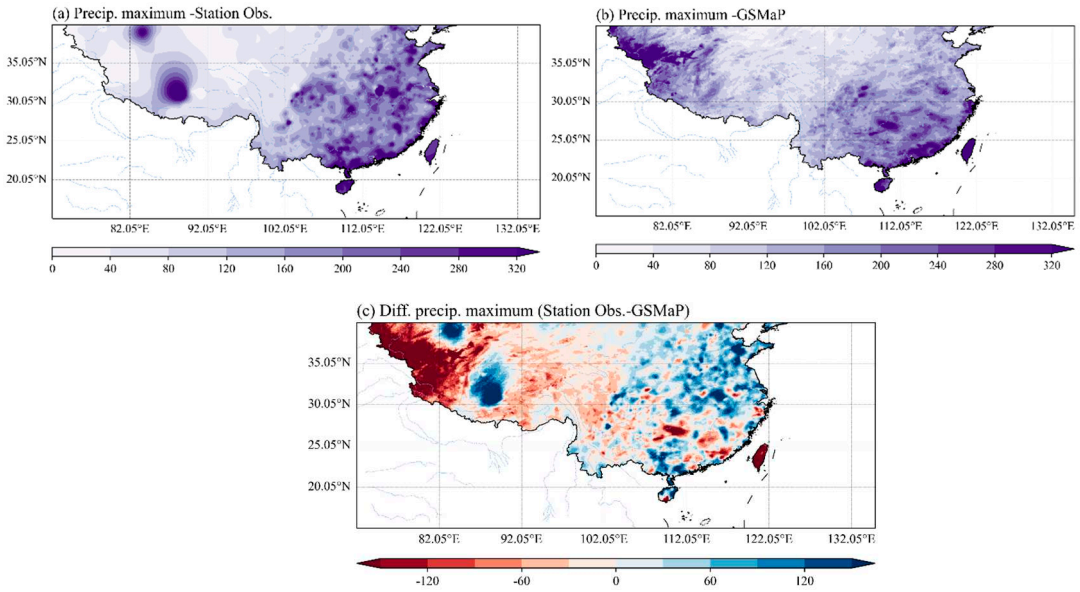

Preprints (www.preprints.org) | NOT PEER-REVIEWED | Posted: 3 November 2023 doi:10.20944/preprints202311.0169.v1

Figure 10. Distribution of annual precipitation maximum across China based on station observations (a, unit: mm) and GSMaP data (b, unit: mm), and biases between station observations and GSMaP data (c, unit: mm) (Station observations minus GSMaP data).

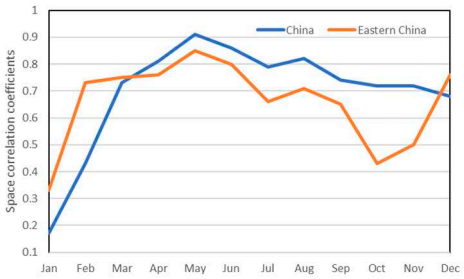

Figure 11. Spatial correlation coefficients of monthly precipitation maximum averaged over China (blue line, 72.05°-122.55°E/17.55°-39.95°N) and eastern China (orange line, 105.05°-122.55°E/17.55°-39.95°N) between station observations and GSMaP data.

For both China and eastern China, there are some differences in the annual cycle of precipitation maximum presented by GSMaP data and station observations (Figure 12). In station observations, the evolution shows an increase from January to July, followed by a decrease. In contrast, GSMaP data exhibits a much smoother variation. Precipitation maximum in GSMaP is greater than in station observations at the beginning and end of the year, but the opposite is true in the middle of the year.

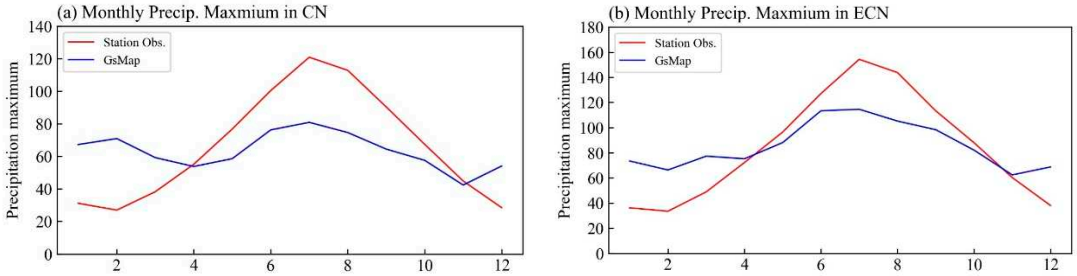

Figure 12. Climatological monthly precipitation maximum averaged over China (a, unit: mm) and eastern China (b, unit: mm) based on station observations and GSMaP data.

3.2. Comparison of climate variability

To validate the ability of GSMaP to depict the climate variability of precipitation in China, annual precipitation, number of rainy days, number of rainstorm days and daily precipitation are averaged over Chian and eastern China from 2001 to 2020 using GSMaP and station observations, respectively. As shown in Figure 13a and 13c, annual precipitation and the number of rainstorm days in China present coherent interannual variation, with correlation coefficients are both up to 0.76, exceeding the confidence level of 99.9%. The correlation of precipitation maximum in China between the two datasets is 0.46, exceeding the confidence level of 95%. However, inconsistencies become more apparent after the early 2010s (Figure 13d). The temporal variation of the number of rainy days in China is less consistent between the two datasets, with a correlation only -0.16 (Figure 13b). It is noteworthy that all four precipitation indices show an obvious difference in magnitude between GSMaP and station observations, indicating that GSMaP generally underestimates the precipitation in China. This observation aligns with the findings in the climatological comparisons. Similar patterns are observed for eastern China. GSMaP and station observations demonstrate highly coherent interannual variation in annual precipitation, the number of rainstorm days and precipitation maximum, with correlations of 0.83, 0.80 and 0.66, respectively, exceeding the confidence level of 99%. However, the opposite variation in the number of rainy days between the two datasets is significant (Figure 13d). In eastern China, the differences in the magnitude of precipitation indices decrease significantly. Notably, the annual precipitation based on the two

Preprints (www.preprints.org) | NOT PEER-REVIEWED | Posted: 3 November 2023 doi:10.20944/preprints202311.0169.v1

datasets is almost identical before the early 2010s. Therefore, it is reasonable to conclude that the underestimation of precipitation by GSMaP mainly occurs in western China.

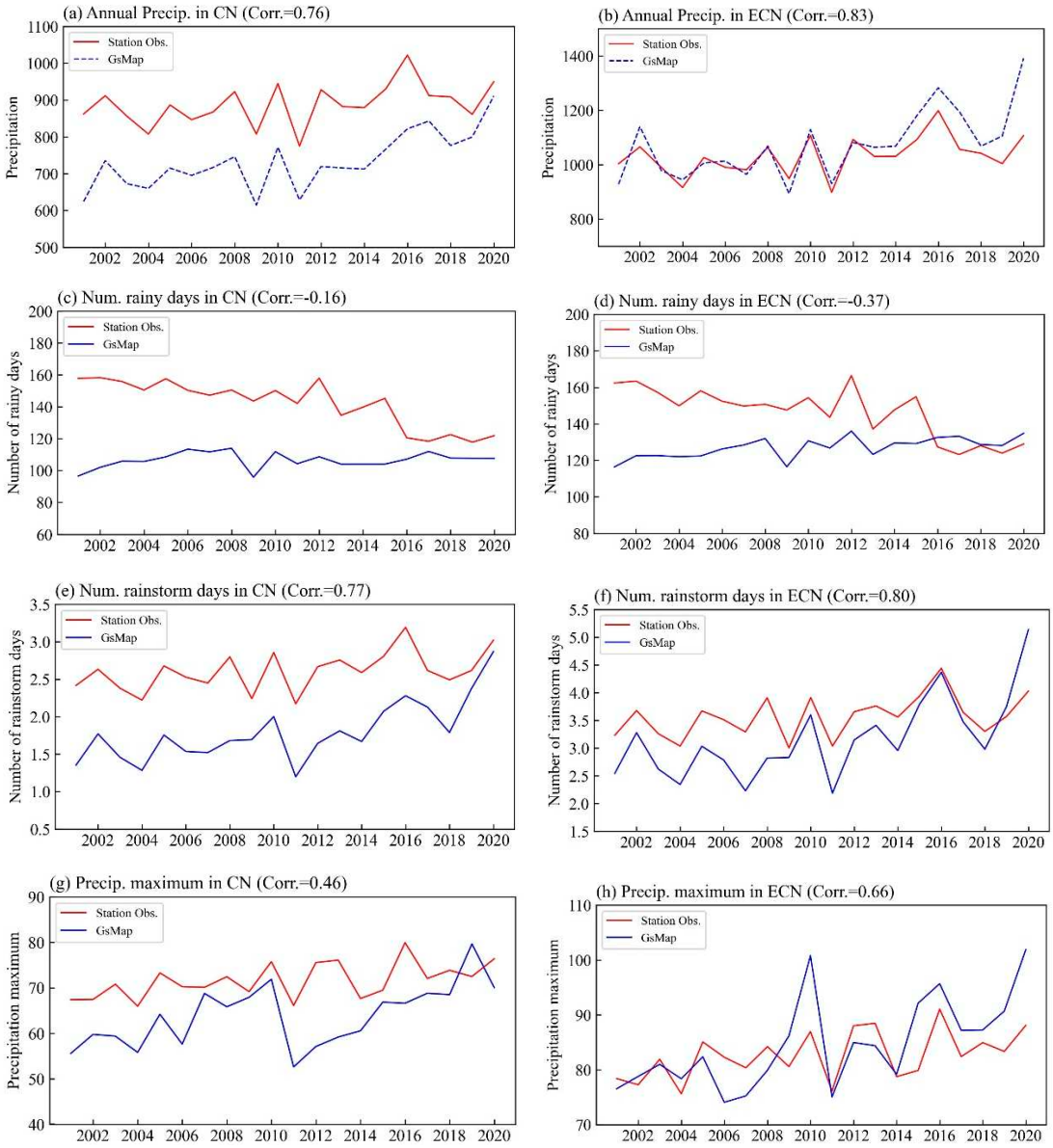

Figure 13. Time series of annual precipitation (a and b, unit: mm), number of rainy days (c and d, unit: days), number of rainstorm days (e and f, unit: days) and precipitation maximum (g and h, unit: mm) across China (a, c, e, g) and eastern China (b, d, f, h) from 2001 to 2020 based on station observations and GSMaP data.

Figure 14 presents the monthly correlations of temporal evolution for each precipitation index between GSMaP data and station observations. It is obvious that the consistency of annual precipitation between the two datasets is the highest, with correlations all above 0.6 and reaching 0.92 (Figure 14a). Moreover, the temporal variation in annual precipitation is more coherent in eastern China than in the whole of China. GSMaP data also well depicts the interannual variation in number of rainstorm days and precipitation maximum, with higher consistency in eastern China, where the correlation coefficients are generally higher (Figure 14c and 14d). The minimum correlation is above 0.4, while the maximum correlation reaches 0.91. It can also be observed that the coherence of interannual variation between the two datasets is higher in the latter half of the year. GSMaP does not capture the interannual variation of the number of rainy days as well (Figure 14b). Its correlations with station observations in Jun and July are notably lower and even opposite for China, with the

Preprints (www.preprints.org) | NOT PEER-REVIEWED | Posted: 3 November 2023 doi:10.20944/preprints202311.0169.v1

maximum correlation being only 0.52 in October. The situation improves in eastern China, especially in the latter half of the year, when the correlations are consistently above 0.6.

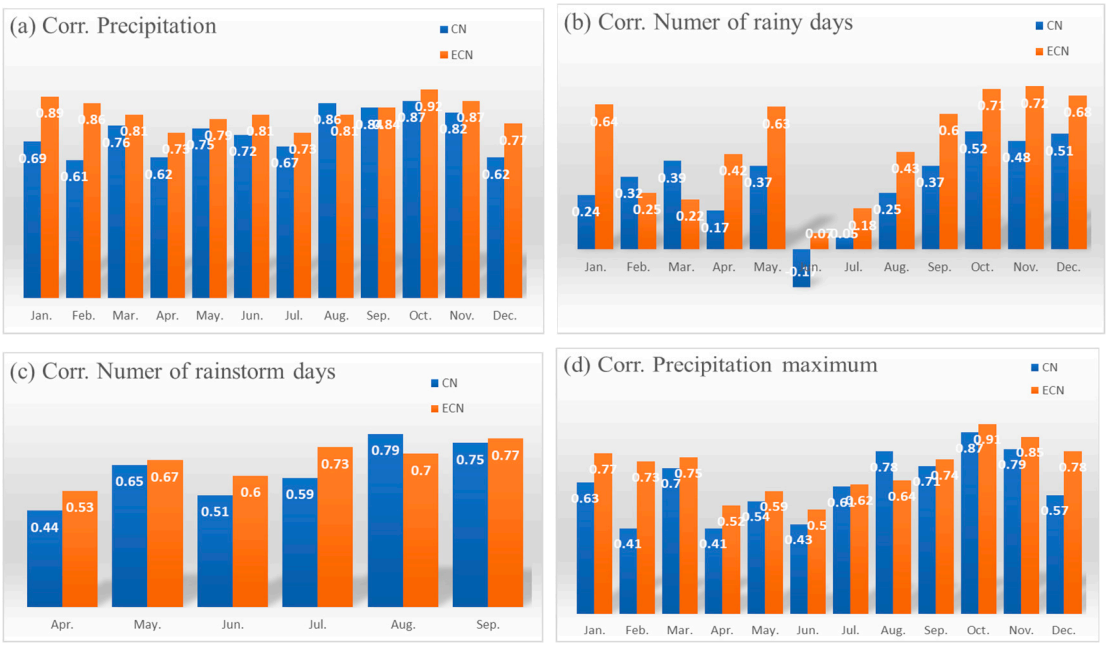

Figure 14. Correlation coefficients of monthly precipitation (a, unit: mm), number of rainy days (b, unit: days), number of rainstorm days (c, unit: days) and precipitation maximum (d, unit: mm) averaged over China and eastern China between station observations and GSMaP data.

In addition to interannual variation, a linear trend can be observed in the time series of precipitation indices from 2001 to 2020. Annual precipitation, the number of rainstorm days and precipitation maximum consistently illustrate an increasing trend by GSMaP and station observations. All three indices show varying degrees of increase, with GSMaP data indicating an acceleration in the increasing trend after the early 2010s However, for the number of rainy days, GSMaP data and station observations present opposite changing trends, with an increasing trend in the former and a decreasing trend in the latter (Figs. 13c and 13d). The linear trend coefficients for the four precipitation indices are calculated month by month (Figure 15). There is a significant difference in the trend of the number of rainy days between GSMaP data and station observations, and they are even opposite in some months. The increasing trend dominates in GSMaP data, while the number of rainy days in China and eastern China consistently shows a decreasing trend each month. For the other three precipitation indices, the changing trends are generally consistent both in China and eastern China, but the magnitude is much greater in GSMaP. It is evident that GSMaP overestimates the increasing trend in precipitation to varying degrees.

Preprints (www.preprints.org) | NOT PEER-REVIEWED | Posted: 3 November 2023 doi:10.20944/preprints202311.0169.v1

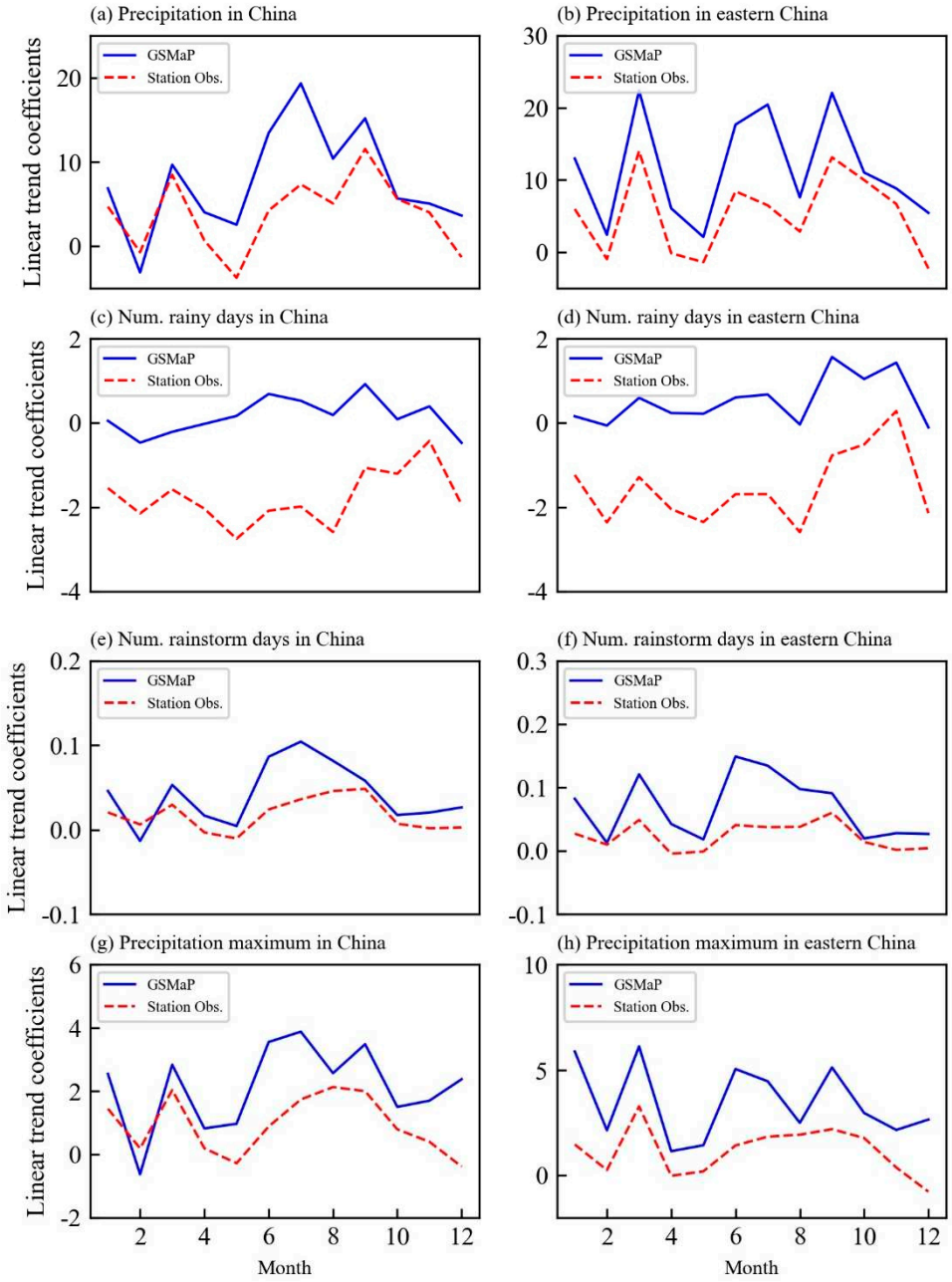

Figure 15. Linear trend coefficients of monthly precipitation averaged over China (a, unit: mm/decade) and eastern China (b, unit: mm/decade) based on station observations and GSMaP data.

4. Discussions

The reliability of GSMaP data in presenting the spatial distribution and temporal variation of precipitation in China has been previously validated by numerous studies [61–64]. In this analysis, its consistency is further affirmed through long-term records and extensive station observations for comparison. However, attention should be directed towards biases, which are critical for both data application and data improvement.

Firstly, a notable overestimate is observed over the Tibetan Plateau for all four precipitation indices. Due to the unique terrain and the absence of reference data from station observations, estimating precipitation on the Tibetan Plateau is a challenge and involves certain uncertainties [76–78]. The same challenges are encountered in other mountainous and plateau areas.

 doi:10.20944/preprints202311.0169.v1

Secondly, a conspicuous increasing trend is observed in the number of rainy days averaged over China. However, many previous studies have highlighted a decrease in rainy days but an increase in precipitation intensity in China [79–81]. The biases in light rainfall estimates by the GSMaP data may contribute to this discrepancy [61,82,83]. Therefore, there is room for improvement in the GMaP' ability to identify whether precipitation occurs and estimate precipitation of different intensities.

Thirdly, the GSMaP data should be applied to climate change research with caution, considering its tendency to overestimate increasing trends in precipitation indices. Efforts should be taken to investigate the potential causes of excessive increase observed after the early 21st century.

5. Conclusions

The GSMaP data provides global precipitation estimates with high spatial and temporal resolution. Numerous previous studies have delved into its reliability in monitoring precipitation in diverse regions. Due to a limited understanding of GSMaP's capacity to depict the climatology and climate variability of various precipitation indices, this study compares the spatial and temporal characteristics of four indices-accumulated precipitation, number of rainy days, number of rainstorm days and precipitation maximum-in China, as derived from GSMaP-GNRT6, with those based on 2419 station observations from 2001 to 2020.

The GSMaP-GNRT6 data generally well captures the spatial distribution of the four precipitation indices in China. The spatial correlations between the GSMaP data and station observations are above 0.7 in most months, particularly for the number of rainstorm days, where the spatial correlations exceed 0.8 in each month over both China and eastern China. Notably, the GSMaP data depicts the spatial distribution of annual precipitation averaged over eastern China better than that over China. Conversely, for the other three indices, the GSMaP data performs better in accurately depicting the spatial distribution over the entire country. However, there are slight limitations in accurately depicting the spatial distribution of the number of rainy days from July to September and precipitation maximum during wintertime over eastern China, showing relatively low spatial correlation in these periods.

The GSMaP data effectively captures the annual cycle of all four precipitation indices, characterized by an increase from the beginning to the middle of the year and a decrease from the middle to end of the year. There is a general underestimation observed in the four precipitation indices averaged over China, but the biases vary across different regions. The accumulated precipitation and number of rainy days are mainly underestimated in the western part of China, while the number of rainstorm days derived from the GSMaP data is less than that observed by station observations over both eastern and western China. The GSMaP data depicts a smoother annual cycle in precipitation maximum compared to station observations, with similar monthly precipitation maximum averaged over China.

The GSMaP demonstrates a strong ability to represent the interannual variation of accumulated precipitation, the number of rainstorm days, and precipitation maximum, particularly for the former two indices, where the correlation coefficients with station observations exceed 0.75. However, a noticeable discrepancy in the interannual variation of the number of rainy days in China between the two datasets is evident. Similarly, accumulated precipitation, the number of rainstorm days, and precipitation maximum based on the GSMaP exhibit a consistent increasing trend comparable to that observed by station observations. Nevertheless, the GSMaP data tends to overestimate this upward trend, especially entering the early 21st century. Regarding the number of rainy days in China, an opposite changing trend is observed between the GSMaP data and station observations, with an upward trend in the former and a downward trend in the latter.

Author Contributions: Conceptualization, Z.W.; methodology, Z.W.; formal analysis, Z.W.; investigation, Q.L.; resources, Z.W.; data curation, Z.W.; writing—original draft preparation, Z.W.; writing—review and editing, Z.W. and Q. L.; visualization, Z.W.; supervision, Z.W.; project administration, Q.L.; funding acquisition, Q.L. All authors have read and agreed to the published version of the manuscript.

Funding: This research is supported by the National Key Research and Development Program of China (2022YFE0136000) and the National Natural Science Foundation of China (U2242207) .

Data Availability Statement: The data from 2419 meteorological stations in China are available from the National Meteorological Information Center of the China Meteorological Administration at **http://data.cma.cn/**. The GSMaP-GNRT6 data is provided by the Japan Aerospace Exploration Agency (JAXA) **https://earth.jaxa.jp/en/data/index.html**.

Acknowledgments: We acknowledge the World Meteorological Organization for initiating the "Space-based Weather and Climate Extremes Monitoring (SWCEM)" project and triggering this analysis. The Japan Aerospace Exploration Agency (JAXA) is appreciated for providing the data. We would like to appreciate Dr. Yuri Kuleshov from the National Climate Center, Australian Bureau of Meteorology for his invaluable recommendations and unwavering support.

Conflicts of Interest: The authors declare no conflict of interest.

References

1. Schär, C.; Frei, C. Orographic precipitation and climate change. *Global change and mountain regions: an overview of current knowledge*, **2005**, 255-266.
2. Douben, K. J. Characteristics of river floods and flooding: a global overview, 1985–2003. *Irrig. Drain.* **2006**, 55(S1), S9-S21.
3. Petley, D. Global patterns of loss of life from landslides. *Geology* **2012**,40, 927–957.
4. Hirabayashi, Y.; Mahendran, R.; Koirala, S.; Konoshima, L.; Yamazaki, D.; Watanabe, S.; Kim, H.; Kanae, S. Global flood risk under climate change. *Nature. Clim. Change* **2013**, 3, 816–821.
5. Dowling, C. A.; Santi, P. M. Debris flows and their toll on human life: a global analysis of debris-flow fatalities from 1950 to 2011. *Nat. Hazards* **2014**, 71, 203–27.
6. Yang, T. H.; Gong, D. H.; Chin, C. T.; Jui, Y. H. Using rainfall thresholds and ensemble precipitation forecasts to issue and improve urban inundation alerts. *Hydrol. Earth Syst. Sci*. **2016**, 20, 4731.
7. Li, x.; Rankin, C.; Gangrade, S.; Zhao, G.; Lander, K.; Voisin N.; Shao, M.; Morales-Hernández, M.; Kao, S. C.; Gao, H. Evaluating precipitation, streamflow, and inundation forecasting skills during extreme weather events: A case study for an urban watershed. *J. Hydrol.* **2021**, 603, 127126.
8. Trenberth, K. E. The impact of climate change and variability on heavy precipitation, floods, and droughts. *Encyclopedia of hydrological sciences*, **2005**, 17, 1-11.
9. Dai, A. Drought under global warming: a review. *Wiley Interdisciplinary Reviews: Climate Change* **2011**, 2(1), 45-65.
10. Mukherjee, S.; Mishra, A.; Trenberth, K. E. Climate change and drought: a perspective on drought indices. *Current climate change reports* **2018**, 4, 145-163.
11. Dai, A.; Zhao, T.; Chen, J. Climate Change and Drought: a Precipitation and Evaporation Perspective. *Curr. Clim. Change* **2018**, 301–312.
12. Wang, Z.; Zhang, Q.; Sun, S.; Wang, P. Interdecadal variation of the number of days with drought in China based on the standardized precipitation evapotranspiration index (SPEI). *J. Clim*. **2022**, 35(6), 2003-2018.
13. Tebaldi, C.; Hayhoe, K.; Arblaster, J. M.; Meehl, G. A. Going to the extremes. *Clim. Change* **2006**, 79 185–211.
14. Schmidt, S.; Kemfert, C.; Höppe, P. The impact of socio-economics and climate change on tropical cyclone losses in the USA. *Reg. Environ. Change* **2010**, 10, 13–26.
15. Stocker, T.; Qin, D.; Plattner, G.; Tignor, M.; Allen, S.; Boschung, J.; Nauels, A.; Xia, Y.; Bex, V.; Midgley, P. *Climate change 2013: the physical science basis: Working Group I contribution to the Fifth assessment report of the Intergovernmental Panel on Climate Change* (Cambridge: Cambridge University Press). **2013**, 167-178.
16. Mullan, D.; Favis-Mortlock, D.; Fealy, R. Addressing key limitations associated with modelling soil erosion under the impacts of future climate change. *Agric. For. Meteorol.* **2012**, 156, 18–30.
17. Woodward, G.; Bonada, N.; Brown, L. E.; Death, R. G.; Durance, I.; Gray, C.; Hladyz, S.; Ledger, M. E.; Milner, A. M.; Ormerod, S. J. The effects of climatic fluctuations and extreme events on running water ecosystems. *Phil. Trans. R. Soc. B* **2016**, 371, 20150274.
18. Paerl, H. W.; Crosswell, J. R.; Van, D. B.; Hall, N. S.; Rossignol, K. L.; Osburn, C. L.; Hounshell, A. G.; Sloup, R. S.; Harding, L. W. Two decades of tropical cyclone impacts on North Carolina's estuarine carbon, nutrient and phytoplankton dynamics: implications for biogeochemical cycling and water quality in a stormier world. *Biogeochemistry* **2018**, 141, 307–332.
19. Allen, M. R.; Ingram, W. J. Constraints on future changes in climate and the hydrologic cycle. *Nature* **2002**, 419, 228–232.
20. Santer, B. D.; Mears, C.; Wentz, F.; Taylor, K.; Gleckler, P.; Wigley, T.; Barnett, T.; Boyle, J.; Brüggemann, W.; Gillett, N. Identification of human-induced changes in atmospheric moisture content. *Proc. Natl Acad. Sci.* **2007**, 104, 15248–15253.

21. Min, S. K.; Zhang, X.; Zwiers, F. W.; Hegerl, G. C. Human contribution to more-intense precipitation extremes. *Nature* **2011**, 470, 378–381.
22. Roderick, T. P.; Wasko, C.; Sharma, A. Atmospheric moisture measurements explain increases in tropical rainfall extremes. *Geophys. Res. Lett.* **2019**, 46, 1375–1382.
23. Tan, X.; Wu, X.; Liu, B. Global changes in the spatial extents of precipitation extremes. *Environ. Res. Lett.* **2021**, 16(5), 054017.
24. Arkin, P. A.; Ardanuy, P. E. Estimating climatic-scale precipitation from space: A review. J. Clim. **1989**, 2(11), 1229-1238.
25. Trenberth, K. E.; Dai, A.; Rasmussen, R. M.; Parsons, D. B. The Changing Character of Precipitation. *Bull. Am. Meteor. Soc.* **2003**, 84, 1205–1217.
26. Daly, C.; Halbleib, M.;Smith, J. I.; Gibson, W. P.; Doggett, M. K.; Taylor, G. H.; Curtis, J.; Pasteris, P. P. Physiographically sensitive mapping of climatological temperature and precipitation across the conterminous United States. *Int. J. Climatol.* **2008**, 28, 2031–2064
27. Michaelides, S.; Levizzani, V.; Anagnostou, E.; Bauer, P.; Kasparis, T.; Lane, J. E. Precipitation: measurement, remote sensing, climatology and modeling, *Atmos. Res*., 2009, 94, 512–533.
28. Stephens, G. L.; L'Ecuyer, T.; Forbes, R.; Gettelmen, A.; Golaz, J. C.; Bodas-Salcedo, A.; Suzuki, K.; Gariel, P.; Haynes, J. Dreary state of precipitation in global models. *J. Geophys. Res. Atmos.* **2010**, 115, D24.
29. Kidd, C.; Levizzani, V. Status of satellite precipitation retrievals. *Hydrol. Earth Syst. Sci*. **2011**, 15, 1109–1116.
30. Tapiador, F. J.; Turk, F. J.; Petersen, W.; Hou, A. Y.; García-Ortega, E.; Machado, L. A. T.; Angelis, C. F.; Salio, P.; Kidd, C.; Huffman, G. J.; Castro, M. Global precipitation measurement: Methods, datasets and applications. *Atmos. Res*., **2012**, 104–105.
31. Sun, Q.; Miao, C.; Duan, Q.; Ashouri, H., Sorooshian, S.; Hsu, K. L. A review of global precipitation data sets: Data sources, estimation, and intercomparisons. *Rev. Geophy*. **2018**, 56(1), 79-107.
32. Beck, H. E.; Vergopolan, N.; Pan, M.; Levizzani, V.; Dijk, A. I. J. M.; Weedon, G. P.; Brocca, L.; Pappenberger, F.; Huffman, G. J.; Wood, E. F. Global-scale evaluation of 22 precipitation datasets using gauge observations and hydrological modeling. *Satellite Precipitation Measurement*. **2020**, 2, 625-653.
33. Xie, P.; Arkin, P. A. Global precipitation: A 17-year monthly analysis based on gauge observations, satellite estimates, and numerical model outputs. *Bull. Amer. Meteor. Soc.* **1997**, 78(11), 2539-2558.
34. Kidd, C. Satellite rainfall climatology: A review. *Int. J. Climatol.* **2001**, 21(9), 1041–1066.
35. Sturaro, G. A. Closer look at the climatological discontinuities present in the NCEP/NCAR reanalysis temperature due to the introduction of satellite data. Clim. Dyn. **2003**, 21, 309–316.
36. Bengtsson, L.; Hagemann, S.; Hodges, K. I. Can climate trends be calculated from reanalysis data?, *J. Geophys. Res.* **2004**, 109.
37. Kalnay, E.; Kanamitsu, M.; Kistler, R.; Collins, W.; Deaven, D.; Gandin, L.; Iredell, M.; Saha, S.; White, G.; Woollen, J.; Zhu, Y.; Chelliah, M.; Ebisuzaki, W.; Higgins, W.; Janowiak, J.; Mo, K. c.; Ropelewski, C.; Wang, J.; Leetmaa, A.; Reynolds, R.; Jenne, R.; Joseph, D. (1996). The NCEP/NCAR 40-year reanalysis project. *Bull. Amer. Meteor. Soc*. **1996**, 77(3), 437–471.
38. Kanamitsu, M.; Ebisuzaki, W.; Woolen, J.; Yang, S. K.; Hnilo, J. J.; Fiorino, M.; Potter, G. L. NCEP–DOE AMIP-II Reanalysis (R-2). *Bull. Amer. Meteor. Soc.* **2002**, 83(11), 1631–1643
39. Uppala, S. M.; KÅllberg, P. W.; Simmons, A. J.; Andrae, U.; Bechtold, V. D. C.; Fiorino, M.; … Woollen, J. The ERA-40 re-analysis. *Quart. J. Roy. Meteor. Soc*. **2005**, 131(612), 2961–3012.
40. Dee, D. P.; Uppala, S. M.; Simmons, A. J.; Berrisford, P.; Poli, P.; Kobayashi, S.; … Vitart, F. The ERA-Interim reanalysis: Configuration and performance of the data assimilation system. Quarterly *Quart. J. Roy. Meteor. Soc*. **2011**, 137(656), 553–597.
41. Hersbach, H.; Bell, B.; Berrisford, P.; et al. The ERA5 global reanalysis. *Quart. J. Roy. Meteor. Soc*. **2020**, 146(730), 1999-2049.
42. Bell, B.; Hersbach, H.; Simmons, A.; Berrisford, P.; Dahlgren, P.; Horányi, A.; Muñoz-Sabater, J.; Nocolas, J.; Radu, R.; Schepers, D.; Soci, C.; Villaume, S.; Bidlot, J. R.; Haimberger, L.; Woollen, J.; Buontempo, C.; Th épaut, J. H. The ERA5 global reanalysis: Preliminary extension to 1950. *Quart. J. Roy. Meteor. Soc*. **2021**, 147(741), 4186-4227.
43. Saha, S.; Moorthi, S.; Pan, H. L.; Wu, X.; Wang, J.; Nadiga, S.; Tripp, P., Kistler, R.; Woollen, J.; … Goldberg, M. The NCEP climate forecast system reanalysis. *Bull. Amer. Meteor. Soc.* **2010**, 91(8), 1015-1058.
44. Saha S, Moorthi S, Wu X, Wang, J.; Nadiga, S.; Tripp, P.; Behringer, D.; Hou, Y. T.; Chuang, H.; … Becher, E. The NCEP climate forecast system version 2. *J. clim.* **2014**, 27(6), 2185-2208.
45. Ebita, A.; Kobayashi, S.; Ota, Y.; Moriya, M.; Kumabe, R.; Onogi, K.; … Ishimizu, T. The Japanese 55-year Reanalysis "JRA-55": An interim report. *SOLA*, **2011**, 7, 149–152.
46. Tashima, T.; Kubota, T.; Mega, T.; Ushio, T.; Oki, R. Precipitation Extremes Monitoring Using the Near-Real-Time GSMaP Product. *IEEE Journal of Selected Topics in Applied Earth Observations and Remote Sensing*, **2020**, 13, 5640-5651.

47. Joyce, R. J.; Janowiak, J. E.; Arkin, P. A.; Xie, P. CMORPH: A method that produces global precipitation estimates from passive nicrowave and infrared data at high spatial and temporal resolution. *J. Hydro.* **2004**, 5, 487–503.
48. Huffman, G. J.; Bolvin, D. T.; Nelkin, E. J.; Wolff, D. B.; Adler, R. F.; Gu, G.; … Stocker, E. F. The TRMM Multisatellite Precipitation Analysis (TMPA): Quasi-global, multiyear, combined-sensor precipitation estimates at fine scales. *J. Hydro.* **2007**, 8(1), 38–55.
49. Hong, Y.; Hsu, K. L.; Sorooshian, S.; Gao, X. G. Precipitation estimation from remotely sensed imagery using an artificial neural network cloud classification system. *J. Appl. Meteor.* **2004**, 43(12), 1834–1852.
50. Hsu, K. L.; Gao, X. G.; Sorooshian, S.; Gupta, H. V. Precipitation estimation from remotely sensed information using artificial neural networks. *J. Appl. Meteor.* **1997**, 36(9), 1176–1190.
51. Sorooshian, S.; Hsu, K. L.; Gao, X.; Gupta, H. V.; Imam, B.; Braithwaite, D. Evaluation of PERSIANN system satellite-based estimates of tropical rainfall. *Bull. Amer. Meteor. Soc.* **2000**, 81(9), 2035–2046.
52. Ushio, T.; Kachi, M. Kalman filtering applications for global satellite mapping of precipitation (GSMaP). In M. Gebremichael & F. Hossain (Eds.), *Satellite rainfall applications for surface hydrology*, **2010**, 105–123). New York: Springer.
53. Kubota, T.; Aonashi, K.; Ushio, T.; Shige, S.; Takayabu, Y. N.; Kachi, M.; Arai, Y.; Tashima, T.; Makaki, T.; Kawamoto, N.; Mega, T.; Yamamoto, M. K.; Hamada, A.; Yamaji, M.; Liu G.; Oki, R. Global Satellite Mapping of Precipitation (GSMaP) products in the GPM era. *Satellite Precipitation Measurement* **2020**, 1, 355-373.
54. Herold, N.; Behrangi, A.; Alexander, L. V. Large uncertainties in observed daily precipitation extremes over land. *J. Geophys. Res. Atmos.* **2017**, 122(2), 668-681.
55. Sekaranom, A. B.; Masunaga, H. Origins of heavy precipitation biases in the TRMM PR and TMI products assessed with CloudSat and reanalysis data. *J. Appl. Meteor. Climatol.* **2019**, 58(1), 37-54.
56. Masunaga, H.; Schröder, M.; Furuzawa, F. A.; Kummerow, C.; Rustemeier, E.; Schneider, U. Inter-product biases in global precipitation extremes. *Environ. Res. Lett.* **2019**, 14(12), 125016.
57. Hou, A. Y.; Kakar, R. K.; Neeck, S.; Azarbarzin, A. A.; Kummerow, C. D.; Kojima, M.; Oki, R.; Nakamura, K.; Iguchi, T. The global precipitation measurement mission. *Bull. Amer. Meteor. Soc.* **2014**, 95(5), 701-722.
58. Skofronick-Jackson, G.; Petersen, W. A.; Berg, W.; Kidd, C.; Stocker, E. F.; Krischbaum, D. B.; Kakar, R.; Braun, S. A.; Huffman, G. J.; Iguchi, T.; Kirstetter, P. E.; Kummerow, C.; Meneghini, R.; Oki, R.; Olson, W. S.; Takayabu, Y. N.; Furukawa, K.; Wilheit, T. The Global Precipitation Measurement (GPM) mission for science and society. *Bull. Amer. Meteor. Soc.* **2017**, 98(8), 1679-1695.
59. Setiawati, M. D.; Miura, F.; Aryastana, P. Validation of Hourly GSMaP and ground base estimates of precipitation for flood monitoring in Kumamoto, Japan. *Geospatial technology for water resource applications*, **2016**, 130-143.
60. Tian, Y.; Peters-Lidard, C. D.; Adler, R. F.; Kubota, T.; Ushio, T. Evaluation of GSMaP precipitation estimates over the contiguous United States. *J. Hydro.* **2010**, 11(2), 566-574.
61. Chen, Z.; Qin, Y.; Shen, Y.; Zhang, S. Evaluation of global satellite mapping of precipitation project daily precipitation estimates over the Chinese mainland. *Adv. Meteor.* **2016**, 2016.
62. Ning, S.; Song, F.; Udmale, P.; Jin, J.; Thapa, B. R.; Ishidaira, H. Error analysis and evaluation of the latest GSMap and IMERG precipitation products over Eastern China. Adv. Meteor. **2017**, 2017.
63. Lu, D.; Yong, B. A preliminary assessment of the gauge-adjusted near-real-time GSMaP precipitation estimate over Mainland China. *Remote Sens.* **2020**, 12(1), 141.
64. Zhou, Z.; Guo, B.; Xing, W.; Zhou, J.; Xu, F.; Xu, Y. Comprehensive evaluation of latest GPM era IMERG and GSMaP precipitation products over mainland China. *Atmos. Res.* **2020**, 246, 105132.
65. Chua, Z. W.; Kuleshov, Y.; Watkins, A. Evaluation of satellite precipitation estimates over Australia. *Remote Sens.* **2020**, 12(4), 678.
66. Setiyoko, A.; Osawa, T.; Nuarsa, I. W. Evaluation of GSMaP precipitation estimates over Indonesia. *Int. J. Environ. Geosci*, **2019**, 3, 26-43.
67. Kuleshov, Y.; Kurino, T.; Kubota, T.; Tashima, T.; Xie, P. "WMO space-based weather and climate extremes monitoring demonstration project (SEMDP): First outcomes of regional cooperation on drought and heavy precipitation monitoring for Australia and South-East Asia", [online] Available: https://www.intechopen.com/books/rainfall-extremes-distribution-and-properties/wmo-space-based-weather-and-climate-extremes-monitoring-demonstration-project-semdp-first-outcomes-o.
68. Zheng, D.; Yao, T. D. Research progress on formation and evolution of Qinghai-Tibet Plateau and its environmental and resource effects (in Chinese). *Chinese Basic Science*, **2004**, 6, 15-21.
69. Ding, Y.; Chan, J. C. L. The East Asian summer monsoon: an overview. *Meteor. Atmos. Phys.* **2005**, 89(1-4), 117-142.
70. Shi, X. Y.; and Shi, X. H. Climatological characteristics of summertime moisture budget over the southeast part of Tibetan Plateau with their impacts (in Chinese). *J. Appl. Meteor. Sci.* **2008**, 19, 41-46.
71. Ding, Y.; Wang, Z. A study of rainy seasons in China. *Meteor. Atmos. Phys.* **2008**, 100(1-4), 121-138.

72. Immerzeel, W. W.; Beek, L. P. V.; Bierkens, M. F. Climate change will affect the Asian water towers. *Science*, **2010**, 328, 1382-1385.
73. Chen, J.; Huang, W.; Jin, L.; Chen, J.; Chen, S.; Chen, F. A climatological northern boundary index for the East Asian summer monsoon and its interannual variability. *Sci. China Earth Sci*. **2018**, 61, 13-22.
74. Xu, X. D.; Dong, L. L.; Zhao, Y.; Wang, Y. J. Effects of the Asian Water Tower over the Qinghai-Tibet Plateau and the characteristics of atmospheric water circulation (in Chinese). *Chin. Sci. Bull.* **2019**, 64, 2830-2841.
75. Chen, J.; Huang, W.; Feng, S.; Zhang, Q.; Kuang, X.; Chen, J. The modulation of westerlies-monsoon interaction on climate over the monsoon boundary zone in East Asia. *Int. J. Climatol*. **2021**, 41, 3049-3064.
76. Zhu, Z.; Yong, B.; Ke, L.; Wang, G.; Ren, L.; Chen, X.Tracing the error sources of global satellite mapping of precipitation for GPM (GPM-GSMaP) over the Tibetan Plateau, China. *IEEE Journal of Selected Topics in Applied Earth Observations and Remote Sensing*, **2018**, 11(7), 2181-2191.
77. Li, Q.; Wei, J.; Yin, J.; Qiao, Z.; Peng, W.; Peng, H. Multiscale comparative evaluation of the GPM and TRMM precipitation products against ground precipitation observations over Chinese Tibetan Plateau. *IEEE Journal of Selected Topics in Applied Earth Observations and Remote Sensing*, **2020**, 14: 2295-2313.
78. Jiang, Y.; Yang, K.; Li, X.; Zhang, W.; Shen, Y.; Chen, Y.; Li, X. Atmospheric simulation - based precipitation datasets outperform satellite - based products in closing basin - wide water budget in the eastern Tibetan Plateau. *Int. J. Climatol*. **2022**, 42(14), 7252-7268.
79. Song, Y.; Achberger, C.; Linderholm, H. W. Rain-season trends in precipitation and their effect in different climate regions of China during 1961–2008. *Environ. Res. Lett.* **2011**, 6(3), 034025.
80. Liu, B.; Chen, C.; Lian, Y.; Chen, J.; Chen, X. Long-term change of wet and dry climatic conditions in the southwest karst area of China. *Glob. Planet. Change*, **2015**, 127, 1-11.
81. Shang, H.; Xu, M.; Zhao, F.; Tijjani, S. B. Spatial and temporal variations in precipitation amount, frequency, intensity, and persistence in China, 1973–2016. *J. Hydro*. **2019**, 20(11), 2215-2227.
82. Shawky, M.; Moussa, A.; Hassan, Q. K.; El-Sheimy, N. et al. Performance assessment of sub-daily and daily precipitation estimates derived from GPM and GSMaP products over an arid environment. *Remote Sens*. **2019**, 11(23), 2840.
83. Lu, D.; Yong, B. Evaluation and hydrological utility of the latest GPM IMERG V5 and GSMaP V7 precipitation products over the Tibetan Plateau. *Remote Sens*. **2018**, 10(12), 2022.